Available online at www.sciencedirect.com
SCIENCE DIRECT
Journal of Colloid and Interface Science 287 (2005) 534–541
JOURNAL OF Colloid and Interface Science
www.elsevier.com/locate/jcis

Formation and characterization of different ceria/silica composite materials via dispersion of ceria gel or soluble ceria precursors in silica sols

Kamal M.S. Khalil *, Leena A. Elkabee, Brian Murphy

Department of Chemistry, College of Science, UAE University, P.O. Box 17551, Al-Ain, United Arab Emirates

Received 6 November 2004; accepted 14 February 2005

Available online 13 April 2005

Abstract

Composite ceria/silica materials of 10 and 20% (w/w) were prepared by calcination, at 650 °C for 3 h, of the xerogels obtained by mixing the corresponding amount of a ceria precursor with freshly prepared sols of spherical silica particles (Stöber particles) in their mother liquors. Two different ceria precursors were examined in this investigation. The first was a gel produced by the prehydrolysis of cerium(IV) isopropoxide in isopropanol medium, and the second was an aqueous solution of cerium(IV) ammonium nitrate. Different textural and morphological characteristics that developed by calcination were investigated by TGA, FTIR, XRD, SEM, and analyses of N_2 adsorption isotherms. The results indicated that ceria dispersion and formation of mesoporous textural composite materials produced by the second precursor, cerium(IV) ammonium nitrate, are better than those produced by the first precursor, prehydrolyzed cerium(IV) isopropoxide. The results are discussed in terms of the effect of precursors and mixing media on nucleation and growth of ceria particles and their protection from sintering on calcination at the test temperature.

Keywords: Sol–gel; Ceria/silica; CeO_2/SiO_2; Thermal stability; Adsorption isotherms; Mesoporous materials

1. Introduction

The main catalytic function of ceria in its catalytic applications is to provide oxygen buffering capacity during a catalytic reaction in which a rich or poor air/fuel ratio arises [1]. The efficiency of ceria in this respect is excellent due to its ability to be reduced from CeO_2 to CeO_{2-x}, where $0 < x < 0.25$ on heating in the range ~330–930 °C, while preserving its structure [2]. The reduction of ceria and its interaction with hydrogen under different conditions have been extensively studied and critically reviewed [1,3]. It was found that the reduction of ceria, which occurs at temperatures higher than 330 °C, is dependent largely on texture [4–6]. Moreover, the effect of the structural and textural aspects of ceria has been reported for many catalytic ceria systems [7–11].

It has been found [2] that doping of ceria with silica or zirconia [2,12,13] induces important structural transformations, which depend on the amount of dopant and on the thermal history of the samples. Rocchini et al. [14] found that under some specific conditions, silica positively affects the redox behavior of ceria, resulting in enhancement of its reduction properties due to the formation of a new phase/compound, $Ce_{9.33}(SiO_4)_6O_2$, the arrangement of which induces stabilization of small ceria crystallites. Formation of this phase enables the limitations imposed by thermodynamics in the reduction of ceria to be overcome,

* Corresponding author. Permanent address: Department of Chemistry, Faculty of Science, South Valley University, P.O. Box 82524, Sohag, Egypt. Fax: +971 3 7671 291 (at UAE).
E-mail address: kamalk@uaeu.ac.ae (K.M.S. Khalil).

0021-9797/$ – see front matter
doi:10.1016/j.jcis.2005.02.041

and almost 80% of cerium formally shifts to the +3 oxidation state in the form of cerium silicate. On reoxidation, this phase decomposes, giving amorphous silica and small ceria crystallites, which are much more reactive toward reduction and oxidation, respectively.

There is much evidence that when ceria is mixed with silica, or silica is used as a support, the overall function of the catalyst improves; e.g., SiO_2 is an effective surface area-stabilizing agent for ceria [15,16]. Ceria-promoted Pt, Rh, or Pd/SiO_2 catalysts were found to be more active than the unpromoted catalyst [17]. Moreover, for Pt/ceria-supported catalysts, Pt was found to diffuse into ceria at room temperature under vacuum and may form Pt–Ce bonds at elevated temperatures. However, the encapsulation effect was not observed for Pt/ceria-promoted SiO_2 catalysts [18].

Despite the advantageous textural and morphological nature of ceria/silica composite materials, their methods of preparation have not been fully explored. Bensalem et al. [19] found that impregnation of SiO_2 with Ce-acetylacetonate led to smaller ceria particles (1–3 nm), as compared with impregnation with a Ce-nitrate precursor (5–9 nm). Cracium [17] has also investigated and compared CeO_2/SiO_2 materials prepared by incipient wetness and grafting. He found that large crystallites, or mostly amorphous CeO_2/SiO_2, were generated by incipient wetness and grafting after calcination at 500 °C. The microstructure evolution of nanocrystalline CeO_2 supported on amorphous SiO_2 on heat treatment in air or in hydrogen, has also been examined [20].

This article describes the preparation of ceria/silica materials by the mixing of a prehydrolyzed cerium(IV) isopropoxide (gel), or cerium(IV) ammonium nitrate aqueous solution, with freshly prepared Stöber silica sols. The aim is to take advantage of the highly dense phase (Stöber silica particles) as a matrix for ceria particles to produce thermally stabilized textural ceria/silica materials. Structural and textural characteristics of the dried materials (uncalcined), as well as the materials produced by calcination for 3 h at 650 °C (calcined), were explored by TGA, FTIR, XRD, SEM, and N_2 adsorption techniques.

2. Experimental

2.1. Materials

Cerium(IV) isopropoxide, $Ce[OCH(CH_3)_2]_4{\cdot}C_3H_7OH$, powder, was a product from Alfa Aesar; cerium(IV) ammonium nitrate $(NH_4)_2Ce(NO_3)_6$ (CAN), solid, a product from Aldrich Chemical Company; tetraethyl orthosilicate, 98% $Si(OC_2H_5)_4$ (TEOS), liquid, a product from Sigma–Aldrich Company, Ltd., Germany. Isopropanol >99.7%, $(CH_3)_2CHOH$ (water content <0.05%), a product of Merck, and aqueous ammonia solution (25% NH_3), 99.99%, also a product of Merck, were used as received.

2.1.1. Preparation of the pure silica material

Pure silica materials were prepared by the Stöber method [21]. A 19.0-ml volume of TEOS was added to 207.0 ml of absolute alcohol, and hydrolysis was initiated by the addition of 155 ml of ammonia (within 1 min) with magnetic stirring (400 rpm), resulting in the formation of Stöber silica sol. The sol was maintained under constant stirring for 1 h. The resultant solution was aged 1 week. The cake that was distilled was filtered off and then dried overnight at 60 °C, followed by further drying at 120 °C for 24 h. The resultant material is termed *uncalcined pure silica*. Portion of the uncalcined material was calcined at 650 °C for 3 h. The calcined material was named calcined pure silica after its precursor.

2.1.2. Preparation of ceria/silica materials from cerium(IV) isopropoxide

Silica supported with 10 and 20% ceria from cerium(IV) isopropoxide (CIP) was prepared as follows. A calculated amount of CIP corresponding to 10 or 20% (w/w ceria/silica) was dispersed in 50 ml of isopropanol (water content <0.05%) with the aid of ultrasonic radiation in a conventional small bench-top ultrasonic bath for 10 min. This led to dispersion and hydrolysis of CIP and subsequent formation of the gel. The resultant gel was transferred into a beaker containing freshly prepared Stöber silica sol produced by the method described above. The solution was magnetically stirred at ca. 400 rpm. The sol was stirred for 1 h. The resultant solution was aged one week, filtered off, and dried, as was the pure silica. The resultant materials derived from the cerium alkoxide precursor (abbreviated Alk) are labeled *uncalcined 10% Alk* and *20% Alk* ceria/silica, respectively. Portions of the uncalcined materials obtained by the method described above were calcined at 650 °C for 3 h. Calcined materials were named after their respective precursors as *calcined 10% Alk* and *20% Alk* ceria/silica, respectively.

2.1.3. Preparation of ceria/silica materials from cerium(IV) ammonium nitrate

Silica supported with 10 and 20% ceria was prepared from cerium(IV) ammonium nitrate (CAN) as follows. A calculated amount of CAN corresponding to 10 or 20% (w/w ceria/silica) was dispersed in 50 ml of doubly distilled water. The resultant solution was transferred into a beaker containing freshly prepared Stöber silica sol produced by the method described above. The solution was magnetically stirred at ca. 400 rpm. The solution was maintained under constant stirring for 1 h. The resultant solution was aged one week, filtered off, and dried as described above. The resultant materials derived from the CAN precursor as a soluble inorganic precursor (abbreviation Ing) are labeled *uncalcined 10% Ing* and *20% Ing* ceria/silica, respectively. Portions of the uncalcined materials obtained by the method described above were calcined at 650 °C

for 3 h. Calcined materials were named after their respective precursors as *calcined 10% Ing* and *20% Ing* ceria/silica, respectively.

2.2. Characterization

2.2.1. Thermogravimetric analysis (TGA)

TGA was carried out using a thermogravimetric analyzer, TA Instruments GA 2950 (USA). A ceramic sample boat was used. Samples weighing 10.0 ± 0.1 mg were heated in a ceramic sample boat up to 700 °C at 10 °C min^{-1} in a stream (40 ml min^{-1}) of nitrogen gas or air.

2.2.2. Fourier transform infrared (FTIR) spectroscopy

FTIR spectra of the samples were obtained using a Fourier transform infrared spectrophotometer, Nicolet FTIR Magna-IR 560 system (USA), in the range 4000–400 cm^{-1}, with 40 scans and a resolution of 4 cm^{-1}.

2.2.3. X-ray diffraction (XRD)

XRD patterns were obtained using a Philips 1840 diffractometer at room temperature. Diffraction patterns were obtained with Ni-filtered CuK_α radiation ($\lambda = 0.154056$ nm). The patterns obtained were matched with standard data for CeO_2, Card No. 34-394 [22], for the purpose of phase identification. The crystallite size of the ceria phase was estimated from the Scherrer equation [23]: $D = (0.9\lambda)/(\beta \cos\theta)$, where D is the crystallite size, λ is the wavelength of the incident X-ray, θ is the angle of diffraction for the 111 line, and β is the half-width of the peak, which was measured graphically.

2.2.4. Scanning electron microscopy (SEM)

Scanning electron micrographs were obtained using a Jeol microscope, Model JSM-5600. Samples were coated with gold before investigation.

2.2.5. Nitrogen gas adsorption

Nitrogen adsorption/desorption isotherms at 77 K were measured using a Model ASAP 2010 instrument (Micromeritics Instrument Corporation, USA). Prior to measurement, all samples were outgassed for 2 h at 150 °C to 0.1 Pa. The specific surface area, S_{BET}, was calculated by applying the BET equation [24]. The average pore diameter was calculated from the ratio $4V_p/S_{BET}$, where V_p is the specific pore volume. Moreover, porosity distribution was generated by BJH analysis using the indicated instrumental software. Microporosity was assessed from t-plot constructions [25], using the Harkins–Jura correlation [26] for a t plot as a function of normalized pressure, p/p_o. t-Plot surface areas, S_t, were calculated from slope analysis of the t plots according to standard methods. Micropore surface area, S_{mic}, the area corresponding to the gas condensed in micropores, was calculated from the relation $S_{mic} = S_{BET} - S_t$.

3. Results and discussion

3.1. Thermogravimetry

TGA and DTG curves for the uncalcined hydrolysis product of TEOS, pure SiO_2, in an atmospheric flow of nitrogen are shown in Fig. 1. A weight loss of 10.6% was recorded on heating the precursor from room temperature (RT) to 700 °C. The DTG curve (Fig. 1) exhibits four peaks, indicating four weight loss steps. The first, which maximizes at 54 °C with a shoulder at 137 °C, corresponds to a weight loss of 5.92%, and most probably involves desorption of the adsorbed organic solvents and water molecules. The other DTG peaks observed at 200, 310, and 452 °C, respectively, may be attributed to the dehydroxylation of the silica surfaces; see FTIR and XRD results below. TGA for the dried basic hydrolysis product of TEOS in a flow of nitrogen gas has been previously investigated [26]. Accordingly, the weight loss in the nitrogen atmosphere originates mainly from desorption of physically adsorbed water (and/or solvents) and surface dehydroxylation of the silica surfaces [27,28].

Fig. 1 also shows the TGA and DTG curves for uncalcined 10% Alk and 20% Alk CeO_2/SiO_2. Weight losses of 12.3 and 12.0% were recorded on heating from RT to 700 °C, respectively. The curves show that the weight loss is continuous, with the rate generally decreasing over the entire heating range, RT to 700 °C, for the two uncalcined materials. Therefore, no clear peaks are observed for the DTG curve; nevertheless a very weak maximum around 280 °C can be observed in both cases. Comparing the curves obtained for uncalcined 10% Alk and 20% Alk CeO_2/SiO_2 with those obtained for uncalcined SiO_2 indicates that addi-

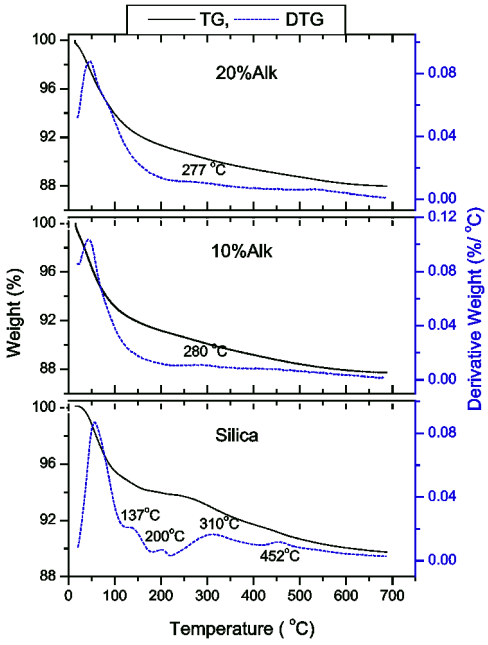

Fig. 1. TGA and DTG curves of the uncalcined hydrolysis products in an atmospheric flow of nitrogen: pure silica, 10% Alk ceria/silica, and 20% Alk ceria/silica.

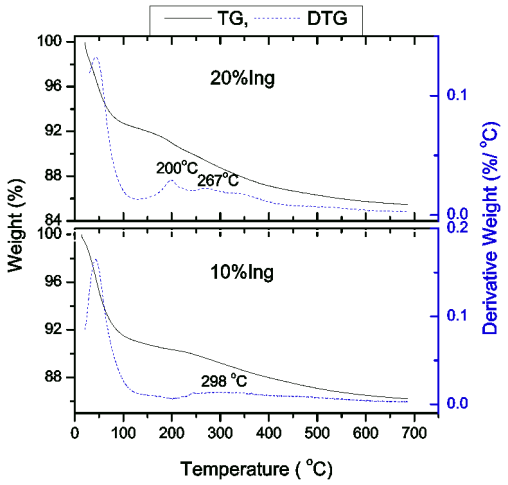

Fig. 2. TGA and DTG curves of uncalcined 10% Ing ceria/silica and 20% Ing ceria/silica materials in an atmospheric flow of nitrogen.

tion of CeO_2 from a prehydrolyzed gel (alkoxide precursor) to SiO_2 sol leads to a small increase in weight loss on heating in the range RT to 700 °C. This slight increase is most probably due to the inclusion or trapping of some more water and solvent molecules in the CeO_2 gel-containing precursors. However, the DTG peaks assigned to the evaporation (of water and/or solvent) and surface dehydroxylation processes for pure uncalcined SiO_2 were not observed for the CeO_2 gel-containing precursors.

Fig. 2 shows the TGA and DTG curves for uncalcined 10% Ing and 20% Ing CeO_2/SiO_2. Weight losses of 13.8 and 14.6% were recorded on heating from RT to 700 °C for the uncalcined 10% Ing and 20% Ing CeO_2/SiO_2, respectively. Fig. 2 shows that the weight loss for uncalcined 10% Ing and 20% Ing CeO_2/SiO_2 is continuous and the general profile is largely similar to the profile observed for pure uncalcined SiO_2. The DTG curves Fig. 2 exhibit a broad peak around 298 °C for uncalcined 10% Ing. However, for uncalcined 20% Ing two peaks appear at 200 and 267 °C. These peaks may be due to the decomposition of the same species related to the inorganic precursor.

3.2. FTIR spectra

Fig. 3a shows the FTIR spectra of pure silica as well as other uncalcined Alk and Ing ceria/silica. The spectrum for uncalcined pure silica exhibits a group of bands that agree with band positions reported for SiO_2 prepared by complete hydrolysis of TEOS, i.e., silica gel [27,29]. Accordingly, the band at 3440 cm^{-1} corresponds to the ν(O–H) mode of (H-bonded) water molecules, the band at 1632 cm^{-1} corresponds to the δ(OH) mode, and the band at 951 cm^{-1} corresponds to ν(Si–OH). The bands at 1100 and 800 cm^{-1} correspond to ν_{as}(Si–O–Si) and ν_s(Si–O–Si) modes, respectively, whereas the band observed at 470 cm^{-1} corresponds to the δ(Si–O–Si) mode. In addition, the weakly intense band at 1384 cm^{-1} may correspond to adsorbed ammonia species.

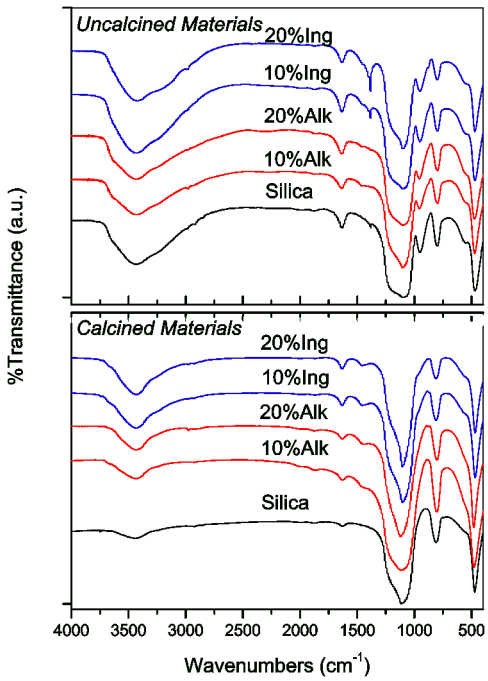

Fig. 3. FTIR spectra of: (a) uncalcined (top), and (b) calcined (bottom) pure silica along with 10% Alk, 20% Alk, 10% Ing, and 20% Ing ceria/silica as indicated.

FTIR spectra for uncalcined 10% Alk and 20% Alk ceria/silica (Fig. 3a) are similar to the spectrum obtained for pure silica. No additional bands are observed. However, the very weak band observed at 1384 cm^{-1} for uncalcined pure SiO_2 is not observed for uncalcined 10% Alk and 20% Alk ceria/silica. FTIR spectra for uncalcined 10% Ing and 20% Ing ceria/silica as shown in Fig. 3a, resemble the spectrum of pure silica. However, the strong band observed at 1384 cm^{-1} for uncalcined 10% Ing and 20% Ing ceria/silica was observed for uncalcined pure silica.

FTIR spectra for calcined pure silica, along with other calcined ceria/silica composite materials, are shown in Fig. 3b. The spectra demonstrate that after calcination at 650 °C for 3 h, all of the peaks previously observed for the uncalcined parent materials appear at the same position, but are of weaker intensity. The weakly intense band observed at 1384 cm^{-1} and the band at 951 cm^{-1} disappeared. This suggests that on calcination, surface dehydration and/or dehydroxylation occurs, as does desorption of any other adsorbed species.

3.3. X-ray diffraction

XRD patterns for uncalcined ceria/silica are shown in Fig. 4a, along with that for the uncalcined silica precursor. The profiles are similar to that for silica. However, for uncalcined 10% Alk and 20% Alk materials only a few broad peaks of high noise/signal ratio are observed at positions close to the characteristic strong lines for ceria (see below), indicating partial crystallization of the dispersed ceria. No

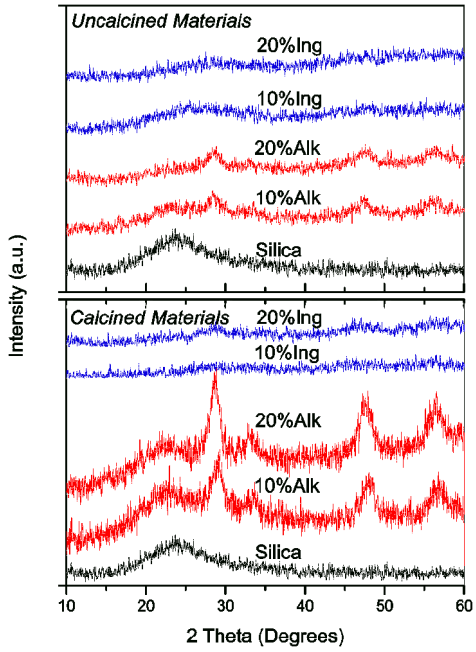

Fig. 4. XRD patterns of: (a) uncalcined (top), and (b) calcined (bottom) pure silica material along with 10% Alk, 20% Alk, 10% Ing, and 20% Ing ceria/silica as indicated.

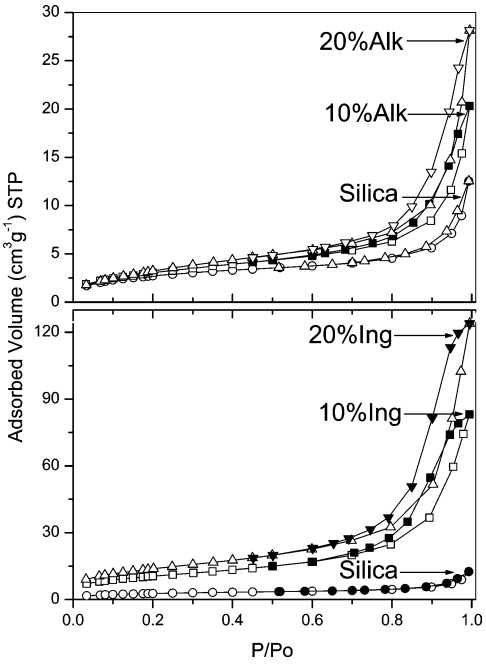

Fig. 5. N_2 adsorption/desorption isotherms for: (a) calcined 10% Alk and 20% Alk ceria/silica along with calcined pure silica (top), and (b) calcined 10% Ing, and 20% Ing ceria/silica along with calcined pure silica (bottom).

similar peaks were observed for uncalcined 10% Ing or 20% Ing materials, which is indicative of their amorphous nature.

XRD patterns for calcined ceria/silica materials, along with patterns for pure silica, are shown in Fig. 4b. The XRD pattern for the calcined silica is one typical of amorphous silica. XRD patterns for calcined 10% Alk and 20% Alk ceria/silica are still dictated by the amorphous-like profile of silica; however, a few broad peaks of high noise/signal ratio are observed at positions very close to the characteristic strong lines for ceria at 28.55°, 47.47°, and 56.33°, respectively, corresponding to the d spacing of 3.12, 1.91, and 1.63 Å characteristic of the (111), (220), and (311) planes of the cerianite (ceria) structure, $Fm3m$ (225). In contrast, XRD patterns for calcined 10% Ing and 20% Ing ceria/silica (Fig. 4b) reflect the amorphous nature of both materials. However, for calcined 20% Ing material, very weak peaks with high noise/signal ratio scarcely can be detected at the characteristic positions for ceria, i.e., close to 28.55°, 47.47°, and 56.33°as indicated above. This result indicates that ceria is present as very finely divided nanosize particles. The crystallite size of ceria was estimated from the Scherrer equation [23] as 13 and 14 nm (±1 nm) for the calcined 10% Alk and 20% Alk composites, respectively. The amorphous nature of the 10% Ing and 20% Ing composites prevent an accurate estimation of the crystallite size. However, more amorphous and much smaller crystallites should be expected for the Ing group than for the Alk group.

3.4. Nitrogen adsorption

Nitrogen adsorption/desorption isotherms for calcined 10% Alk and 20% Alk ceria/silica along with that for calcined pure silica, are shown in Fig. 5a. According to the original IUPAC classification [30], the isotherm for pure calcined silica is rather similar in shape to type II type isotherms with a scarcely obvious narrow loop. The isotherms for 10% Alk and 20% Alk materials exhibit an increase in total pore volume adsorbed near $p/p_0 = 1$, and the hysteresis loops are wider than for pure calcined silica. The isotherms can be classified as type IV (with some contribution from type II) isotherms, and the loops as H3 type hysteresis loops.

Corresponding isotherms for calcined 10% Ing and 20% Ing ceria/silica are shown in Fig. 5b, along with that for calcined pure silica, which is plotted here again for comparative purposes. The isotherms for 10% Ing and 20% Ing materials exhibit a large increase in total pore volume adsorbed near $p/p_0 = 1$, and the hysteresis loops are much wider than those of the 10% Alk and 20% Alk materials. The isotherm can be classified as a type IV isotherm. The hysteresis loops can be classified as H3 (with some properties of H2) hysteresis loops. Additionally, according to the recent classification of adsorption isotherms [31], isotherms obtained with pure silica and with calcined 10% Alk and 20% Alk materials are classified as type IIb isotherms, whereas isotherms obtained with the calcined 10% Ing and 20% Ing materials are classified as mixed type IIb and IVa isotherms.

Textural characteristics including surface area, S_{BET}, external surface area, S_t, micropore area, S_{mic}, and pore width for the test materials are listed in Table 1. The results indicate that calcined 10% Alk and 20% Alk materials scarcely show higher S_{BET} values of 11.3 and 12.7 $m^2\,g^{-1}$, respectively, compared with 10.0 $m^2\,g^{-1}$ for calcined pure silica.

Table 1
Textural characteristics: surface area, S_{BET}, BET constant, c_{BET}, external surface area, S_t, micropore area S_{mic}, and pore diameters for the test materials calcined at 650 °C in air for 3 h

Material	S_{BET} ($m^2\,g^{-1}$)	c_{BET}	S_t ($m^2\,g^{-1}$)	S_{mic} ($m^2\,g^{-1}$)	Pore diameter (nm)	
					Average	BJH
Pure silica	10.0	74.7	3.8	6.2	5.8	11.5
10% Alk ceria/silica	11.3	52.1	7.5	3.8	9.5	12.9
20% Alk ceria/silica	12.7	28.8	8.9	3.8	11.8	14.0
10% Ing ceria/silica	38.3	88.7	34.0	4.4	12.8	15.2
20% Ing ceria/silica	50.5	78.4	46.3	4.2	14.6	16.6

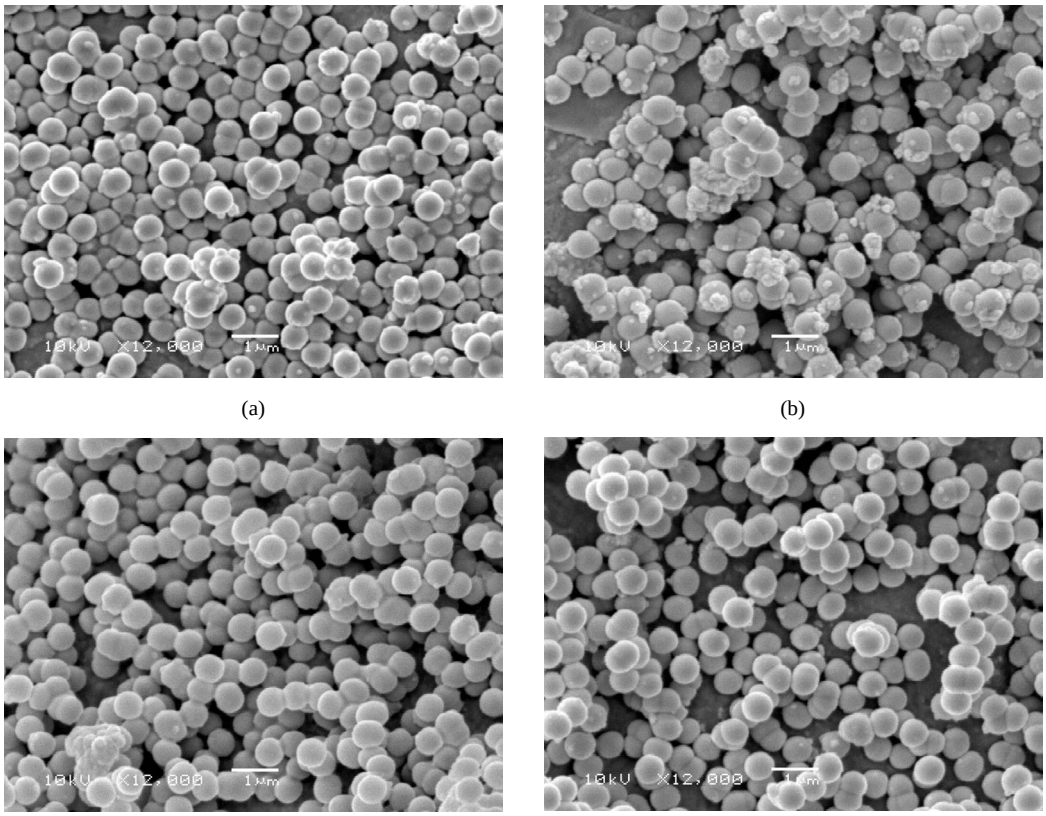

Fig. 6. Scanning electron micrographs of uncalcined ceria/silica materials: (a) 10% Alk, (b) 20% Alk, (c) 10% Ing, (d) 20% Ing.

In addition, lower contributions for microporosity are obtained for calcined 10% Alk and 20% Alk materials (3.8 and 3.8 $m^2\,g^{-1}$, respectively) than for calcined pure silica (6.2 $m^2\,g^{-1}$). Consequently, this gives rise to a higher contribution for the external surface area, S_t, for the indicated materials than for the calcined silica (see Table 1).

Results for calcined 10% Ing and 20% Ing ceria/silica materials clearly have higher surface areas, S_{BET}, of 38.3 and 50.5 $m^2\,g^{-1}$, respectively, compared with 10.0 $m^2\,g^{-1}$ for calcined silica. Moreover, despite this large increase in the S_{BET}, lower S_{mic} values are obtained for the 10% Ing and 20% Ing materials (4.4 and 4.2 $m^2\,g^{-1}$, respectively) than for the calcined silica (6.2 $m^2\,g^{-1}$). This gives rise to higher S_t values of 34.0 and 46.3 $m^2\,g^{-1}$, respectively, for 10% Ing and 20% Ing materials compared with 3.8 $m^2\,g^{-1}$ for calcined silica (see Table 1).

3.5. Scanning electron microscopy

Scanning electron micrographs of the uncalcined materials (Figs. 6a–6d) show the spherical silica particle matrix and the ceria dispersed phase, which appears as smaller irregular particles. The composite produced from the Alk precursor, specifically uncalcined 20% Alk materials, show that ceria particles are aggregating in a variable size aggregate and overall nonuniform dispersion within the silica matrix. However, better dispersion in terms of smaller ceria particles within the matrix is observed for materials produced from the Ing precursor. In addition, better dispersion was found on the uncalcined 10% Ing material than on the 20% Ing material.

Scanning electron micrographs of calcined ceria/silica materials (Figs. 7a–7d) illustrate large morphological differ-

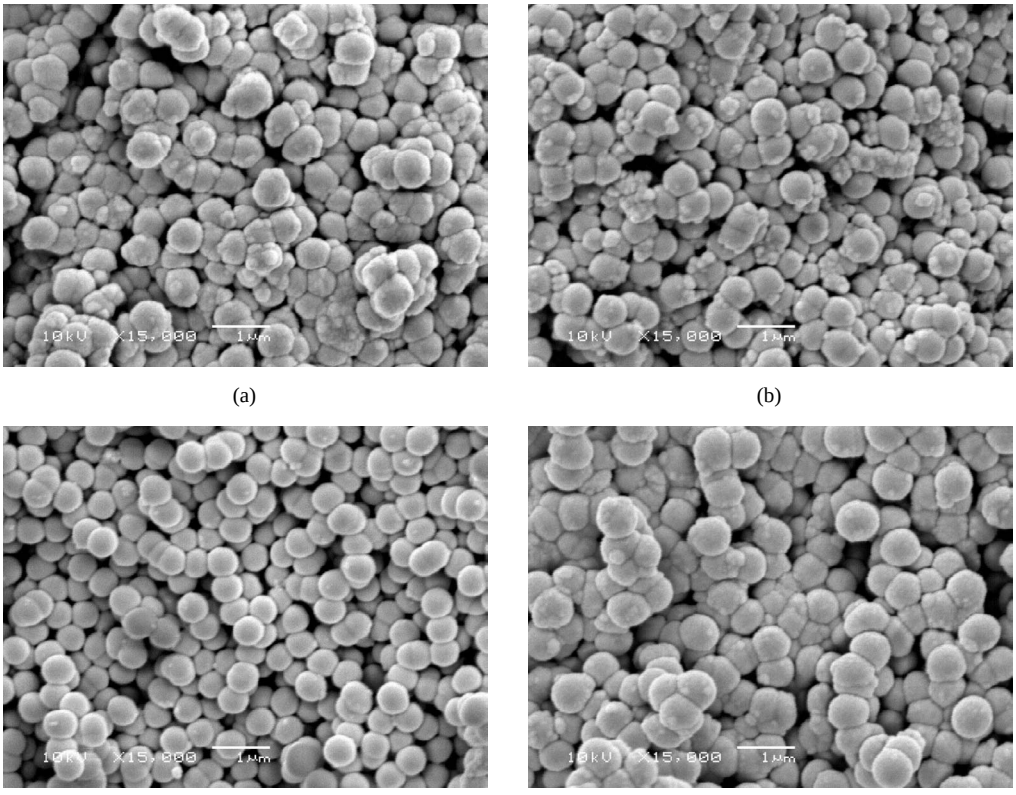

Fig. 7. Scanning electron micrographs of calcined materials: (a) 10% Alk, (b) 20% Alk, (c) 10% Ing, (d) 20% Ing.

ences between the two groups of calcined materials. The Alk group shows a case of sintering in large domains, whereas the Ing group shows a case of open aggregating morphology of less sintering and better porosity. Irregular aggregates of ceria particles, ∼0.1–0.5 μm in diameter, are observable in the Alk group micrographs (Figs. 7a and 7b), whereas smaller aggregates, <0.1 μm in diameter, can be recognized in the Ing group micrographs (Figs. 7c and 7d). In terms of the above XRD results, rather smaller aggregates and/or individual particles should be present in the latter micrographs for the Ing group, as supported by the above XRD results. These observations are in agreement with the S_{BET} and porosity measurements, which indicates low surface areas of 11.3 and 12.7 $m^2\,g^{-1}$, respectively, for the 10% Alk and 20% Alk materials and high surface areas of 38.3 and 50.5 $m^2\,g^{-1}$, respectively, for the 10% Ing and 20% Ing materials. Moreover, the SEM results show the exact morphological difference between the two groups of materials.

The above results indicate that there are essential differences between the Alk and Ing groups of materials. This can be explained in terms of different interactions of the Alk and Ing precursors with silica sol during the preparation. For the Alk precursor, the CeO_2 species was in gel form when it was added to the respective silica particle sol, as the species had been prehydrolyzed by traces of water present in the isopropanol medium during the ultrasonic treatment step. In fact, gelling of the hydrolyzed $Ce(IV)(OPr^i)_4{\cdot}(OPr^i)$ during the ultrasonic dispersion stage was influenced by the limited amount of water present and the high electropositivity of the Ce^{4+} ion. It should be noted that the gel precursor was used because $Ce(IV)(OPr^i)_4{\cdot}(OPr^i)$ itself is not readily soluble in isopropanol. In a recent study, our group investigated pure ceria powders produced via sol–gel processing of the ultrasonically dispersed $Ce(IV)(OPr^i)_4{\cdot}(OPr^i)$ in a neutral or basic medium [32]. Accordingly, textures were porous especially for the materials processed in basic solutions ($S_{BET} = 44.2\ m^2\,g^{-1}$ for the material calcined at 650 °C for 3 h). However, the results of the present study show that there was little opportunity for the gel to redisperse in the silica sol due to the highly basic conditions present in the mother liquor of the sol. The latter factor may lead to further condensation of the surface gel layers, making them much more crosslinked and consequently less available for dispersion. Scanning electron micrographs of the uncalcined 10% Alk and 20% Alk ceria/silica materials support this argument. This explains the presence of the ceria domain within the silica particles for the calcined materials, the formation of the crystalline ceria phase, and why no significant increase in the surface area was observed. However, in the case of another alcohol-soluble metal alkoxide, such as titanium(IV) tetraisopropoxide, it was possible to prepare finally dispersed titania/silica under similar conditions [27]. This indicates that there are differences between alcohol-soluble alkoxide-type precursors and gel alkoxide-type precursors.

However, an inorganic precursor such as cerium(IV) ammonium nitrate may be a good alternative (to replace soluble alkoxide) for the preparation of ceria/silica composites. Results show that when cerium(IV) ammonium nitrate is used as the source of the CeO_2 phase, soluble cerium(IV) ions go through the process of hydrolysis, nucleation, and growth of ceria particles in the mother liquor of the silica sol. Hence, under highly basic conditions, the rate of nucleation is very rapid, whereas the growth rate is slow, in particular if the amount of CeO_2 is limited. Apparently, as indicated by the results obtained, 10 or 20% (w/w) ceria/silica satisfied the conditions required for rapid nucleation and corresponding slow growth rates. This correlates with the observation of finely dispersed ceria particles on the surface of the supporting silica particles as seen in the scanning electron micrographs. Consequently, the presence of such fine particles on the surface of silica particles increases their roughness and allows textural modification, as reflected by highly improved surface area and porosity.

4. Conclusion

It can be concluded that addition of either type of ceria precursor to silica sols leads to the formation of composite materials of modified texture and microstructural details of lower microporosity and higher external surface area. However, the effect is much more pronounced for materials prepared from the inorganic precursor, 10% Ing and 20% Ing composites, than for materials prepared from the gel precursor, i.e., 10% Alk and 20% Alk materials. The results show that there is better dispersion of ceria and formation of mesoporous textural composites by the cerium(IV) ammonium nitrate precursor than by the gel precursor, prehydrolyzed cerium(IV) isopropoxide. These results indicate that ceria from cerium(IV) ammonium nitrate can be dispersed very finely in basic silica sols to produce ceria/silica composites with good textural and thermal characteristics. This approach offers an alternative for metal alkoxides especially, when the latter are insoluble in alcoholic media.

References

[1] E. Rocchini, M. Vicario, J. Llorca, C. de Leitenburg, G. Dolcetti, A. Trovarelli, J. Catal. 211 (2002) 407.
[2] A. Trovarelli, M. Boaro, E. Rocchini, C. de Leitenburg, G. Dolcetti, J. Alloys Compd. 323/324 (2001) 584.
[3] S. Bernal, J.J. Calvino, J.M. Gatica, C. Lopez Cartes, J.M. Pintadoarelli, in: A. Trovarelli (Ed.), Catalysis by Ceria and Related Materials, in: Catalytic Science Series, vol. 2, Imperial College Press, London, 2002, pp. 85–168, chap. 4.
[4] V. Perrichon, A. Laachir, S. Abouarnadasse, O. Touret, G. Blanchard, Appl. Catal. A 129 (1995) 69.
[5] L.A. Bruce, M. Hoang, A.E. Hughes, T.W. Turney, Appl Catal. A 134 (1996) 351.
[6] F. Giordano, A. Trovarelli, C. de Leitenburg, M. Giona, J. Catal. 193 (2000) 273.
[7] H. Vidal, J. Kašpar, M. Pijolat, G. Colon, S. Bernal, A. Cordón, V. Perrichon, F. Fally, Appl. Catal. B 27 (2000) 49.
[8] H. Vidal, J. Kašpar, M. Pijolat, G. Colon, S. Bernal, A. Cordón, V. Perrichon , F. Fally, Appl. Catal. B 30 (2001) 75.
[9] J. Xiaoyuan, L. Guanglie, Z. Renxian, M. Jianxin, C. Yu, Z. Xiaoming, Appl. Surf. Sci. 173 (2001) 208.
[10] R. Cracium, W. Daniell, H. Knözinger, Appl. Catal. A 230 (2002) 153.
[11] G. Sedmak, S. Hocevar, J. Levec, J. Catal. 222 (2004) 87.
[12] J. Kašpar, P. Fornasiero, M. Graziani, Catal. Today 50 (1999) 285.
[13] J. Kašpar, P. Fornasiero, in: A. Trovarelli (Ed.), Catalysis by Ceria and Related Materials, in: Catalysic Science Series, vol. 2, Imperial College Press, London, 2002, pp. 217–241, chap. 6.
[14] E. Rocchini, A. Trovarelli, J. Llorca, G.W. Graham, W.H. Weber, M. Maciejewski, A. Baiker, J. Catal. 194 (2000) 461.
[15] G.-N. Sauvion, J. Caillod, C. Gourlaouen, U.S. patent 4,940,685, 1990.
[16] L. Bonneau, T. Chopin, O. Touret, U.S. patent 5,529,969, 1996.
[17] R. Cracium, Solid State Ionics 110 (1998) 83, and references therein.
[18] Y. Zhou, M. Nakashima, J.M. White, J. Phys. Chem. 92 (1988) 812.
[19] A. Bensalem, F. Bozon-Verduraz, M. Delamar, G. Bugli, Appl. Catal. 121 (1995) 81.
[20] L. Kepinski, M. Wocyrz, M. Marchewka, J. Solid State Chem. 168 (2002) 110.
[21] W. Stöber, A. Fink, E. Bohn, J. Colloid Interface Sci. 26 (1968) 62.
[22] JCPDS, International Centre for Diffraction Data, CD, 1996.
[23] H.P. Klug, L.E. Alexander, X-Ray Diffraction Procedure for Polycrystalline and Amorphous Material, Wiley, New York, 1974.
[24] B. Brunauer, P.H. Emmett, E. Teller, J. Am. Chem. Soc. 60 (1938) 309.
[25] P.A. Webb, C. Orr, Analytical Method in Fine Particle Technology, Micrometrics, Norcross, USA, 1997.
[26] W.D. Harkins, G.J. Jura, J. Chem. Phys. 11 (1943) 431.
[27] K.M.S. Khalil, A.A. Elsamahy, M.S. Elanany, J. Colloid Interface Sci. 249 (2002) 359.
[28] D.C.M. Dutoit, M. Schneider, A. Baiker, J. Catal. 153 (1995) 165.
[29] C.J. Brinker, G.W. Scherer, Sol–Gel Science, the Physics and Chemistry of Sol–Gel Processing, Academic Press, New York, 1989.
[30] K.S.W. Sing, D.H. Everett, R.A.W. Haul, L. Moscou, R.A. Pierotti, J. Rouquerol, T. Siemieniewska, Pure Appl. Chem. 57 (1985) 603.
[31] F. Rouquerol, J. Rouquerol, K. Sing, Adsorption by Powders and Porous Solids, Academic Press, London, 1999.
[32] K.M.S. Khalil, L.A. Elkabee, B. Murphy, Micropor. Mesopor. Mater. 78 (2005) 83.